

# Active Adaptive Battery Aging Management for Electric Vehicles

Matteo Corno  and Gabriele Pozzato 

**Abstract**—The battery pack accounts for a large share of an electric vehicle cost. In this context, making sure that the battery pack life matches the lifetime of the vehicle is critical. The present work proposes a battery aging management framework which is capable of controlling the battery capacity degradation while guaranteeing acceptable vehicle performance in terms of driving range, recharge time, and drivability. The strategy acts on the maximum battery current, and on the depth of discharge. The formalization of the battery management issue leads to a multi-objective, multi-input optimization problem for which we propose an online solution. The algorithm, given the current battery residual capacity and a prediction of the driver's behavior, iteratively selects the best control variables over a suitable control discretization step. We show that the best aging strategy depends on the driving style. The strategy is thus made adaptive by including a self-learned, Markov-chain-based driving style model in the optimization routine. Extensive simulations demonstrate the advantages of the proposed strategy against a trivial strategy and an offline benchmark policy over a life of 200 000 (km).

**Index Terms**—Battery aging management, electric vehicle, optimization.

## ACRONYMS

BMS	Battery Management System
EV	Electric Vehicle
HEV	Hybrid Electric Vehicle
MPC	Model Predictive Control
PSO	Particle Swarm Optimization

## I. INTRODUCTION

IN THE last years, challenges associated with vehicle powertrain modeling, optimization, and control have gained increasing interest. As a matter of fact, tight vehicular emission regulations have led car manufactures to develop new, green, mobility solutions. In this scenario, EV's are considered an effective solution for everyday urban mobility because of the absence of local emissions [1], the low price of electrical energy, and their good performance. The diffusion of EV's is limited by their cost, which is still higher than that of their internal

combustion engine counterpart. The cost of the battery pack and its possible replacement during the lifetime of the vehicle are large factors in the EV's economy. Matching the lifetime of the battery with that of the vehicle is thus an imperative for the success of EV's. To solve this issue, models and operational strategies must be developed to understand, monitor, and control the phenomenon of battery aging.

Li-ion batteries are the principal choice for transportation applications thanks to their high energy and power density [2]. These energy storage devices, as all other batteries, are subject to aging, which leads to capacity loss [3]. Battery aging is generally divided into two principal causes: calendar aging and cycle aging. Calendar aging is the irreversible capacity degradation caused by the battery storage conditions. Calendar aging rate highly varies according to storage temperatures [4] and to the State of Charge (*SoC*). High temperatures lead to secondary reactions such as corrosion, which brings to capacity fade [5]. Conversely, low temperatures lead to battery chemistry alterations [6]. Moreover, according to [3], for an equal storage temperature high *SoC* values lead to higher battery degradation. On the other hand, cycle aging is related to the battery utilization. Since battery cycle aging is caused by complex electrochemical phenomena, studies are typically empirical [7]–[10]. Battery cells are tested under different operating conditions in order to derive semi-empirical models, which relate the battery capacity loss to stress factors such as temperature, *SoC*, and current. Concerning Li-ion batteries, Depth of Discharge (*DoD*), temperature, and C-rate are the principal stress factors affecting cycle aging [2], [3], [11]. For instance, charging and discharging batteries at high *DoD*, high temperatures, and high C-rate accelerate the aging process, as well as having unbalanced cells in a battery pack.

Even though battery aging is a well known issue, controlling the battery degradation over time still remains an open point. Most of the works in this sense have been in the context of Hybrid Electric Vehicles (HEV's) [12]–[14]. In this context, aging is one of the aspects, along with overall efficiency, that the power split logic needs to account for. For example, in [13] and [14] the power split between the available movers, i.e., the internal combustion engine and the battery, is obtained minimizing a performance index accounting for battery aging. Moreover, in [15]–[17] a least costly energy management is proposed. In this scenario, an euro equivalent cost is associated to the battery capacity degradation. The presence of multiple power sources simplifies HEV's aging management: the degree of freedom given by the power split allows one to avoid conditions that are

Manuscript received January 18, 2019; revised May 20, 2019 and August 1, 2019; accepted August 26, 2019. Date of publication November 13, 2019; date of current version January 15, 2020. This work was supported by the Online Accurate Battery State Estimation via Electrochemical Modelling, MIUR SIR project RBSI14STHV. The review of this article was coordinated by Prof. Matthias Preindl. (Corresponding author: Matteo Corno.)

The authors are with the Dipartimento di Elettronica, Informazione e Bioingegneria, Politecnico di Milano, 20133 Milano, Italy (e-mail: matteo.corno@polimi.it; gabriele.pozzato@polimi.it).

Digital Object Identifier 10.1109/TVT.2019.2940033



regulator [24]. Thus, traction torque requests ( $T_m^{req}$ ) are computed based on the difference between the reference, which is the driver's desired longitudinal velocity, and the actual vehicle speed:

$$T_m^{req} = k_p \varepsilon = k_p (v_{ref} - v) \quad (1)$$

with  $k_p$  the proportional gain. The motor current is computed as follows:

$$i_m^{req} = \frac{T_m^{req}}{k_m} \quad (2)$$

where  $k_m$  is the electric motor torque constant. The requested motor current is then saturated to  $I_{max}^1$ , which is computed from the output of the aging management strategy  $I_{max}^{cell}$  according to:

$$I_{max} = f(I_{max}^{cell}, \omega_m, \bar{\eta}_m) = \frac{I_{max}^{cell} V_b n_p}{\omega_m k_m} \bar{\eta}_m, \quad (3)$$

where  $\bar{\eta}_m$  is the electric motor efficiency,  $V_b$  the battery pack voltage,  $n_p$  the number of cells in parallel configuration, and  $\omega_m$  the motor rotational speed. The control variable  $I_{max}^{cell}$  generally limits the battery cell current at the cost of limiting the vehicle acceleration and of increasing the battery recharge time. In Fig. 1, the relationship between  $I_{max}^{cell}$  and  $I_{max}$  is expressed by  $f(\cdot)$ . Starting from the current provided by the motor  $i_m^{sat}$ , the actual vehicle speed is computed according to the vehicle longitudinal dynamics:

$$M\dot{v} = i_m^{sat} \frac{k_m r_t}{R_w} - \frac{1}{2} \rho_a v^2 C_x A - F_r \quad (4)$$

with  $M$  and  $v$  the vehicle mass and speed,  $r_t$  the gear ratio,  $R_w$  the wheel radius,  $F_r$  the rolling resistance,  $C_x$  the drag coefficient,  $\rho_a$  the air density, and  $A$  the vehicle cross sectional area. Therefore, the power provided by the traction motor for the motion is modeled as follows:

$$P_m = \frac{k_m i_m^{sat} v}{R_w r_t} = k_m i_m^{sat} \omega_m = T_m^{sat} \omega_m \quad (5)$$

with  $T_m^{sat}$  the motor torque. In the backward facing portion, the electric machine is modeled as an efficiency map which computes the battery power:

$$P_b = \begin{cases} \frac{P_m}{\eta_m(P_m)}, & \text{if } P_m \geq 0 \text{ (motor)} \\ P_m \eta_m(P_m), & \text{if } P_m < 0 \text{ (generator)} \end{cases} \quad (6)$$

with  $\eta_m$  the motor efficiency. Thus, the cell power request is given by  $P_{cell} = P_b/n_{cell}$  with  $n_{cell} = n_s \times n_p$  the total number of cells of the battery pack and  $n_s, n_p$  respectively the number of cells in series and parallel configuration. In this work, an A123 cylindrical LiFePO<sub>4</sub> cell with a nominal voltage of 3.3 (V) and characterized by a nominal capacity  $Q_{nom} = 2.5$  (Ah) is considered. A series/parallel configuration with  $n_s = 110$  and  $n_p = 26$  is chosen, leading to a total number of cells equal to 2860.

**Charging management.** During the vehicle lifetime, the battery is recharged multiple times, with the charging events generally function of the State of Charge and the geographical

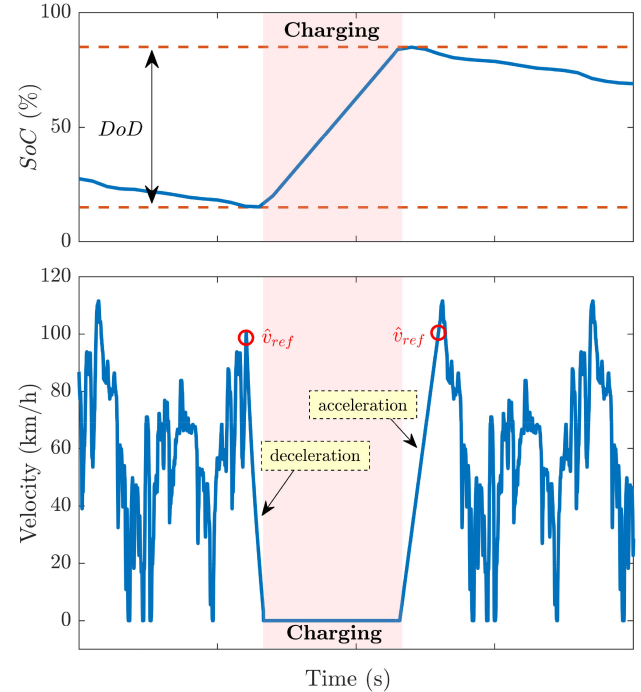


Fig. 2. Charging event. Once the allowed battery  $DoD$  is exploited, the vehicle is decelerated from  $\hat{v}_{ref}$  to 0 (km/h). Then, the vehicle is recharged and accelerated again to a speed  $\hat{v}_{ref}$ , i.e., the desired vehicle speed before the charging event.

position of the charging stations. In this work, fast charging stations are assumed to be always available along the trip. Therefore, as soon as the battery reaches the limit State of Charge, the vehicle is decelerated from the current desired speed  $\hat{v}_{ref}$  to 0 (km/h) and then recharged at a power limited by the maximum cell current  $I_{max}^{cell}$ . Once the charge is completed, the vehicle is accelerated again to  $\hat{v}_{ref}$ . Rather than reasoning in terms of  $SoC$ , the aging strategy employs the  $DoD$  as the control variable. We define the  $DoD$  to be symmetric with respect to a  $SoC$  of 50%. For instance, a  $DoD$  of 70% (Fig. 2) denotes a battery  $SoC$  varying between 15% and 85%. Note that, on the optimization scales of thousands of kilometers, neglecting the exact position of the charging points is reasonable.

## B. Battery Cell Modeling

As pointed out in the introduction, modeling aging phenomena is a complex task, most contributions rely on semi-empirical models. In our framework, we follow the same path in order to design a control-oriented model. The model leverages some simplifying assumptions:

- 1) We assume the presence of a BMS guaranteeing the balancing of all the cells in the battery back;
- 2) We describe an average model that neglects cell polarization;
- 3) Even though temperature is accounted for in the model, we assume the BMS to be equipped with an energy management system.

<sup>1</sup>The capital letter  $I$  denotes quantities expressed in C-rate rather than Ampere.

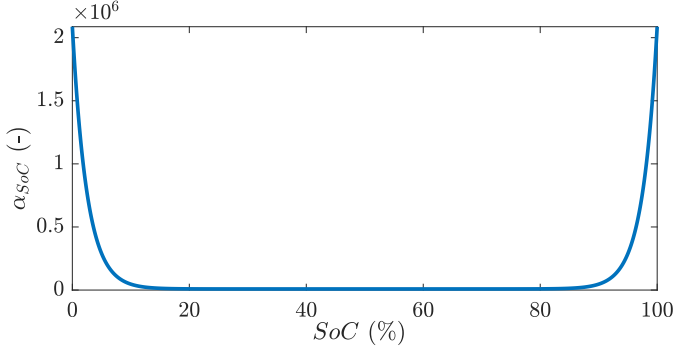


Fig. 3. Battery  $SoC$  penalizing factor. The aging increases exponentially for  $SoC$  values lower than 20% and higher than 80%.

Under these assumptions, the battery pack is modeled as a single large cell with its electrical equivalent circuit: a voltage source  $v_{oc}$  and a resistance  $R_{cell}$  accounting for Joule losses. The battery open circuit voltage is function of the  $SoC$ , while its resistance is generally depending on aging and temperature. Thus, the cell current is given by:

$$i_{cell} = \frac{v_{oc} - \sqrt{v_{oc}^2 - 4R_{cell}P_{cell}}}{2R_{cell}}. \quad (7)$$

The cell  $SoC$  dynamics [26] takes the following expression:

$$S\dot{o}C = -\frac{i_{cell}}{Q} \quad (8)$$

with  $Q$  the cell capacity, decreasing with aging. As already shown in [24], the battery aging model is derived from [9] and extended from the HEV's scenario to the EV's one. Therefore, the rate of capacity loss with respect to the processed  $Ah$  is described as follows:

$$\begin{cases} \frac{dQ}{dAh} = -\frac{z}{100}\alpha_{SoC} \exp\left(\frac{-E_a + \eta|I_{cell}|}{R_g(273.15+T)}\right) Ah^{z-1} \\ \dot{A}h = \frac{1}{3600}|I_{cell}|Q_{nom} \end{cases} \quad (9)$$

with the second equation modeling the  $Ah$  throughput as the total current processed by the cell. The parameters  $E_a$  and  $R_g$  are the activation energy, equal to 31.5 (kJ/mol), and the universal gas constant.  $\eta$  and  $z$  are identified from experimental data.  $\alpha_{SoC}$  is a penalizing factor that accelerates the aging for low and high  $SoC$  [10], [27]:

$$\alpha_{SoC} = d(1 + c e^{b(SoC_{min} - SoC)})(1 + c e^{b(SoC - SoC_{max})}) \quad (10)$$

with  $SoC_{min}$ ,  $SoC_{max}$ ,  $b$ ,  $c$ , and  $d$  empirically determined shaping parameters (Fig. 3). The main stress factors affecting the cell aging behavior are: its  $SoC$ , its temperature  $T$ , and the C-rate  $I_{cell}$ , i.e., the operating current normalized with respect to the nominal cell capacity  $Q_{nom}$ . Battery aging leads also to an increment of the internal resistance. Thus, the following linear relationship between a resistance increment  $\Delta R_{cell}$  and a capacity decrement  $\Delta Q$  is introduced:

$$\Delta R_{cell} = -k_{res}\Delta Q \quad (11)$$

with  $k_{res}$  derived from the experimental data of [28]. Eventually, recalling that the temperature dependency of the cell internal

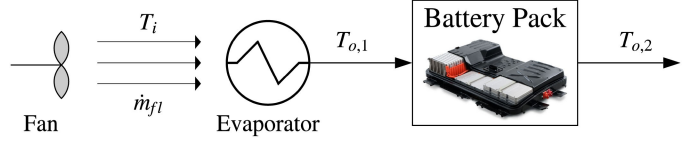


Fig. 4. Battery cooling circuit.

resistance is expressed by [29]:

$$R_{cell}^1 = R_{cell,0} e^{\left(\frac{T_1}{T - T_2}\right)} \quad (12)$$

with  $R_{cell,0}$  the nominal cell resistance and  $T_1$ ,  $T_2$  identified parameters, the following is obtained:

$$R_{cell} = R_{cell}^1 + \Delta R_{cell}. \quad (13)$$

It should be noted that the proposed model is empirical in nature and thus subject to variation depending on the actual characteristic of the cell in use. The framework, while needing an aging model, does not exploit any specific features of the proposed model.

**Thermal management.** Temperature is one of the stress factors increasing battery aging. For this reason, a common practice in automotive companies is to introduce a battery cooling system in order to control the temperature to a desired value  $T$ . Here, we consider an air-cooled battery pack. Fig. 4 depicts the high level architecture. Given  $\dot{m}_{fl}$  the mass flow rate of the air forced by the fan into the cooling system evaporator, the heat exchange is given by:

$$\dot{Q}_{ev} = \dot{m}_{fl} C_{p,fl} (T_i - T_{o,1}) \quad (14)$$

where  $C_{p,fl}$  is the specific heat capacity of air,  $T_i$  and  $T_{o,1}$  the air temperature at the evaporator input and output respectively. Thus, the cooled air is forced into the battery pack, leading to the following energy balance:

$$-\dot{Q}_b = \dot{m}_{fl} C_{p,fl} (T_{o,1} - T_{o,2}) \quad (15)$$

where  $\dot{Q}_b$  is the heat exchange between battery and air, and  $T_{o,2}$  the air temperature after the battery pack. Under the assumption of a uniform temperature distribution  $T$  and modeling the heat generated by the battery pack as  $R_b i_b^2$ ,  $\dot{Q}_b$  is rewritten as follows:

$$\dot{Q}_b = R_b i_b^2 + \frac{T_{room} - T}{R_{conv}} \quad (16)$$

with  $T_{room}$  the room temperature,  $R_b$  the total battery pack resistance,  $i_b$  the battery pack current, and  $R_{conv}$  the thermal resistance between the battery and the surroundings. Assuming no other heat exchange takes place and that  $T_i = T_{o,2}$ , the following equality holds true:

$$\dot{Q}_b = \dot{Q}_{ev}. \quad (17)$$

Therefore, the per-cell electric power absorbed by the cooling circuit, i.e., by the compressor, to control the battery temperature at  $T$  is given by:

$$P_{cool} = \frac{1}{n_{cell} COP} \dot{Q}_{ev} \quad (18)$$



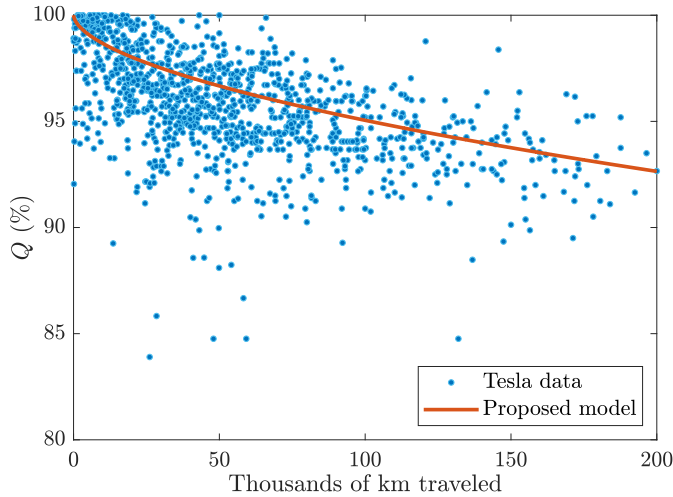


Fig. 5. Comparison of the output of the model against publicly available battery degradation data.

where COP is the coefficient of performance of the cooling system [30]. Eventually, the total power requested to each cell is increased by  $P_{cool}$ , leading to the following equation:

$$P_{cell}^{tot} = P_{cell} + P_{cool}. \quad (19)$$

For further details on battery thermal modeling, the reader is referred to [31], [32].

### C. Model Analysis and Validation

Before setting the formal optimization problem; it is interesting to get a qualitative understanding of the effect of the stress factors on aging.

The proposed EV modeling is validated over 200 thousand kilometers. The simulation is performed considering the driver's desired speed to be modeled as an *Artemis Rural* [33] driving cycle concatenated several times; this driving cycle is a good compromise between urban and highway driving conditions. In this scenario, no active battery aging management is implemented on board and  $I_{max}^{cell} = 2.5$  (C-rate) and  $DoD = 70\%$ . This is a reasonable choice because a  $DoD$  of 70% allows for a satisfactory driving range, while limiting battery aging. Fig. 5 compares the simulated aging against publicly available real life use [34]. In figure, the cell capacity degradation is normalized with respect to the nominal capacity  $Q_{nom}$ . The comparison shows that the open-loop model correctly captures the aging dynamics of real life vehicles. It is worth to mention that the comparison must be regarded as a reasonableness check instead of a rigorous validation. Indeed, due to the lack of battery aging experimental data for the vehicle under investigation, Tesla Model S [34] data are used for the comparative analysis.

The second phase of the analysis studies the effect of the chosen control variables. Fig. 6 plots the aging dynamics for  $I_{max}^{cell} = 2.5$  (C-rate) and three  $DoD$  values (60, 70, and 80%). These simulations confirm the expected non-linear dependency on the  $DoD$ . Fig. 7 simulates the effect of changing  $I_{max}^{cell}$ . In this particular example, the effect of  $I_{max}^{cell}$  on the aging is more linear

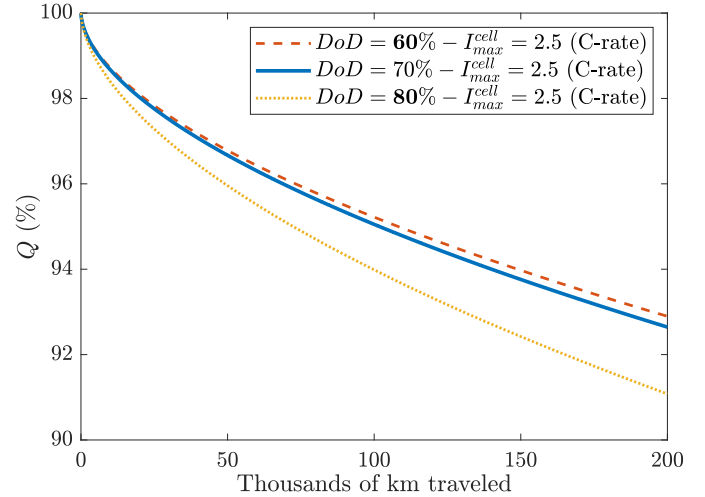


Fig. 6. Effect of the  $DoD$  on the cell capacity. The maximum current is limited to 2.5 (C-rate) and the  $DoD$  is varying between 60% and 80%.

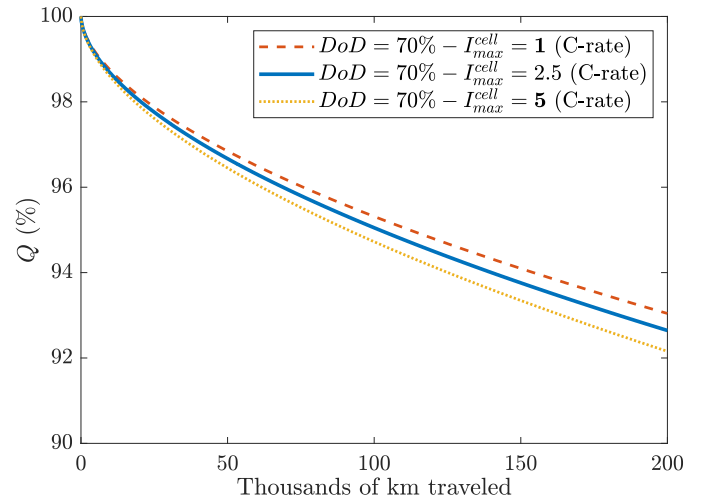


Fig. 7. Effect of the current limitation  $I_{max}^{cell}$  on the cell capacity. The  $DoD$  is fixed at 70% and the  $I_{max}^{cell}$  is varying between 1 (C-rate) and 5 (C-rate).

for a given driving cycle. On the other hand, the effect of  $I_{max}^{cell}$  are more dependent on the driving cycle. The more the desired speed profile is demanding from an acceleration perspective, the more impact  $I_{max}^{cell}$  shows.

### III. DRIVER'S BEHAVIOR LEARNING

The battery aging model shows that the cell current is one of the stress factors to be reckoned with. The cell current heavily depends on the instantaneous driver's torque request. The driving style has an impact on the aging dynamics. This section proposed a model to describe the driver's behavior and a learning mechanism that allows the model to adapt to changes in the driving style. Similarly to [35], [36], the driver actions are modeled by means of a Markov chain stochastic process with states  $\mathcal{W} = \{\mathbf{w}_1, \mathbf{w}_2, \dots, \mathbf{w}_s\} \subseteq \mathbb{R}^2$ , where  $s$  denotes the

number of states. Each state  $\mathbf{w}_m$ , for all  $m \in \{1, \dots, s\}$ , is defined as a couple  $(v_m, a_m)$  with the scalar quantities  $v_m$  and  $a_m$  respectively speed and acceleration. Thus, the driver's behavior is parametrized as transitions from a (velocity, acceleration) pair to another. All the probabilities of transitioning, in one time step, from any state to any other state are summarized in the transition probability matrix  $\mathcal{T} \in \mathbb{R}^{s \times s}$ :

$$\mathcal{T}_{mn} = P(\mathbf{w}(j+1) = \mathbf{w}_n | \mathbf{w}(j) = \mathbf{w}_m) = \lambda_{mn} \quad (20)$$

for all  $n, m \in \{1, \dots, s\}$ .

The transition matrix can be learnt offline or online as new transitions are recorded. It is thus possible to learn the driver's model (i.e., the driver's desired speed) through an online adaptation of (20). Assuming at a time instant  $j+1$  the past and present states to be  $\mathbf{w}_m$  and  $\mathbf{w}_n$  respectively, the probability update is computed as follows [35]:

$$\Delta\lambda_{mn}(j+1) = \bar{\lambda} \sum_{n=1}^s \delta_{mn}(j+1), \quad \text{for all } m \in \{1, \dots, s\} \quad (21)$$

where  $\bar{\lambda} \in \{0, 1\}$  is the probability update magnitude and  $\delta_{mn}(j) = 1$  only when the transition from  $m$  to  $n$  is active, otherwise  $\delta_{mn}(j) = 0$ . Since transition probabilities going out from each node  $\mathbf{w}_m$  must sum up to one, the following update rule is introduced:

$$\mathcal{T}_{mn}(j+1) = (1 - \Delta\lambda_{mn}(j))\mathcal{T}_{mn}(j) + \delta_{mn}(j)\Delta\lambda_{mn}(j+1) \quad (22)$$

for all  $n, m \in \{1, \dots, s\}$ . The initial guess for  $\mathcal{T}$  may be randomly chosen or computed from existing driving cycles, as in [37]. With the proposed approach, at each time instant, the transition probability matrix is updated according to the current and past driver's desired speeds and accelerations. Indeed, assuming the driver's action on the gas pedal to be modeled as in (1), the desired reference speed can be computed from the torque request  $T_m^{req}$  and the actual longitudinal speed  $v$  as follows:

$$v_{ref} = \frac{T_m^{req}}{k_p} + v. \quad (23)$$

Backward Euler differentiation is employed to compute the associated acceleration  $a_{ref}$ . Therefore, the pair  $(v_{ref}, a_{ref})$  defines a state of the Markov chain stochastic process, which can be used to update the transition probabilities. Fig. 8 shows a portion of the transition probability matrix obtained considering the driver's desired speed to be modeled as an *Artemis Rural* driving cycle.

Once a transition probability is known, the desired speed profile can be randomly generated as a realization of the Markov chain. Fig. 9 compares the speed and acceleration distributions of the *Artemis Rural* driving cycle and of a driving cycle generated from the transition probability matrix of Fig. 8, over a traveled distance of 500 (km). From figure, one concludes that the *Artemis Rural* driving cycle and the generated profile are equivalent in terms of speed and acceleration distributions but will be different in terms of time domain behavior.

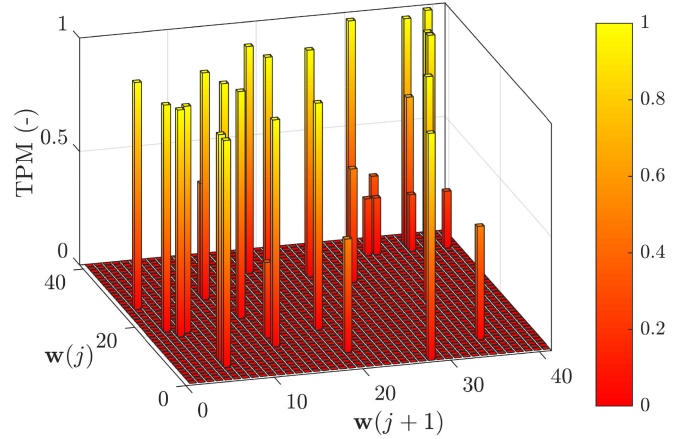


Fig. 8. Portion of the transition probability matrix obtained assuming the driver's desired speed to be modeled as an *Artemis Rural* driving cycle.

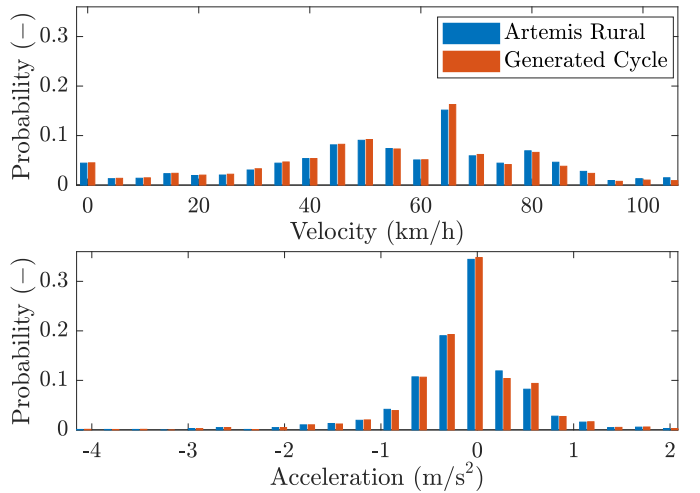


Fig. 9. Velocity and acceleration distributions for the *Artemis Rural* driving cycle and of the driving cycle generated from the transition probability matrix of Fig. 8 are shown.

#### IV. BATTERY AGING MANAGEMENT

This section develops two battery aging management approaches: an offline approach that relies on the perfect knowledge of future driving cycle, and an implementable approach. Both optimization algorithms modulate the *DoD* and the maximum current  $I_{max}^{cell}$  in the attempt of minimizing the capacity degradation while guaranteeing acceptable driving performance in terms of range, charging time, and fulfillment of a desired speed profile.

The performance index  $J$  quantifies the above considerations and translates a multi-objective optimization problem into a single objective one:

$$\begin{aligned} & \underset{\mathbf{u}}{\text{minimize}} && \alpha_l J_{life} + \alpha_s J_{speed} + \alpha_c J_{charge} - \alpha_r J_{range} \\ & \text{subject to} && \end{aligned}$$

$$\begin{cases}
\dot{SoC} = -\frac{i_{cell}}{Q} \\
\frac{dQ}{dAh} = -\frac{z}{100}\alpha_{SoC} \exp\left(\frac{-E_a + \eta|I_{cell}|}{R_g(273.15+T)}\right) Ah^{z-1} \\
\dot{Ah} = \frac{1}{3600}|I_{cell}|Q_{nom} \\
\dot{v} = \frac{1}{M}\left(i_m^{sat}\frac{k_m r_t}{R_w} - \frac{1}{2}\rho_a v^2 C_x A - F_r\right) \\
i_m^{req} = k_p(v_{ref} - v)/k_m \\
I_{max} = f(I_{max}^{cell}, \omega_m, \bar{\eta}_m) \\
i_m^{sat} = \begin{cases} i_m^{req}, & |i_m^{req}| \leq I_{max}Q_{nom} \\ I_{max}Q_{nom}, & i_m^{req} > I_{max}Q_{nom} \\ -I_{max}Q_{nom}, & i_m^{req} < -I_{max}Q_{nom} \end{cases} \\
P_{cell} = P_b(i_m^{sat}, \omega_m)/n_{cell} \\
i_{cell} = \frac{v_{oc} - \sqrt{v_{oc}^2 - 4R_{cell}P_{cell}}}{2R_{cell}} \\
I_{cell} = i_{cell}/Q_{nom} \\
\frac{1 - DoD}{2} \leq SoC \leq 1 - \frac{1 - DoD}{2}
\end{cases} \quad (24)$$

with  $\mathbf{u} = [DoD, I_{max}^{cell}]^T$  the vector of the control variables and  $P_b(i_m^{sat}, \omega_m)$  denoting that the battery power is computed relying on (5) and (6). According to Section II-A, when the  $SoC$  reaches the lower bound the vehicle stops and the battery is recharged. The minus before the last cost component denotes that only  $J_{range}$  must be maximized.

$J$  accounts for several objectives. The first term penalizes the capacity degradation over the traveled kilometers  $\mathcal{N}$ :

$$J_{life} = \frac{Q(0) - Q(\mathcal{N})}{\mathcal{N}} \quad (25)$$

with  $Q(0) = Q_{nom}$  the nominal capacity.

$J_{speed}$  is accounting for the error between the driver's desired speed  $v_{ref}$  and the actual vehicle speed  $v$ :

$$J_{speed} = \sqrt{\frac{1}{t(\mathcal{N})} \int_0^{t(\mathcal{N})} (v_{ref}(\tau) - v(\tau))^2 d\tau} \quad (26)$$

with  $t(\mathcal{N})$  the time horizon, i.e., the time to travel  $\mathcal{N}$  kilometers.

The terms  $J_{charge}$  and  $J_{range}$  respectively take into account the charging time and the driving range:

$$\begin{aligned}
J_{charge} &= \sqrt{\frac{1}{\mathcal{E}(\mathcal{N})} \sum_{i=1}^{\mathcal{E}(\mathcal{N})} t_c(i)^2} \\
J_{range} &= \sqrt{\frac{1}{\mathcal{E}(\mathcal{N})} \sum_{i=1}^{\mathcal{E}(\mathcal{N})} d_r(i)^2}
\end{aligned} \quad (27)$$

where  $\mathcal{E}(\mathcal{N})$  is the total number of charging events over  $\mathcal{N}$ ,  $t_c$  the charging time for each event expressed in minutes, and  $d_r$  the traveled distance between two charging events expressed in kilometers.

In  $J$  the weights  $\alpha_l$ ,  $\alpha_s$ ,  $\alpha_c$ , and  $\alpha_r$  play the important role of balancing out different objectives. Their choice is non-trivial and is discussed next. Changing the  $DoD$  has generally a great impact on the vehicle range,  $J_{range}$ , and on the charging time,

$J_{charge}$ , but in practice no effect on  $J_{speed}$  as long as the battery is operated in the linear region of the open circuit voltage curve. It will become clear later that the control algorithm avoids operating the battery outside this region to prevent excessive aging. Moreover, the bigger the  $DoD$ , the higher the range and the charging time. Conversely, a variation of  $I_{max}^{cell}$  has a negligible impact on the range and affects only the vehicle charging time, limiting the charging current, and  $J_{speed}$ .

### A. Offline Optimization

Given the presence of nonlinearities, the complex modeling structure, the mixing of fast (vehicle motion and  $SoC$ ) and slow (battery aging) dynamics and the dependency on the driving cycle, solving (24) is not trivial. To better understand the features of the problem, first we solve the full knowledge optimization problem. A Particle Swarm Optimization (PSO) [38] approach computes the control actions  $DoD$  and  $I_{max}^{cell}$ . PSO easily deals with nonlinearities in the objective function and in the constraints, proving to be a good candidate algorithm to solve the battery aging management issue.

The optimization problem is posed on a total traveled distance  $\mathcal{N}$  of 200 thousand kilometers, with a control discretization step  $\mathcal{N}_u$  of 10 thousand kilometers. Both the  $DoD$  and the  $I_{max}^{cell}$  are discretized into  $\mathcal{N}/\mathcal{N}_u = 20$  consecutive elements, whose values are selected relying on the PSO algorithm. Given the slow dynamics of the battery aging, the selection of  $\mathcal{N}_u$  is reasonable and it ensures the PSO algorithm to converge in an acceptable time, i.e., two weeks, with a particle swarm size  $p_{\#,1} = 200$ . The optimization procedure is ended when the best objective function value is not changing for 30 consecutive iterations.

Equation (24) merges different objectives in a single cost function. The parameters of that equation represent the trade-off coefficients. In order to better assess and quantify the trade-off, optimizations for a varying coefficient are performed over 200 thousand kilometers considering the *Artemis Rural* driving cycle. In these optimizations, the coefficient  $\alpha_l$  varies between  $5 \times 10^7$  and  $9 \times 10^8$  (km/Ah) while the weights for  $J_{speed}$ ,  $J_{charge}$ , and  $J_{range}$  are equal to:

$$\alpha_s = 100 \text{ (s/m)}, \quad \alpha_c = 1 \text{ (1/min)}, \quad \alpha_r = 1 \text{ (1/km)}. \quad (28)$$

The weights (28) are chosen to make the magnitude of the associated cost components comparable. Moreover, for the problem at hand, varying only  $\alpha_l$  is reasonable because, while managing the battery life, the major concern is monitoring its capacity degradation over time. Thus, Fig. 10 represents the optimization results in terms of components of the cost function. Increasing  $\alpha_l$  allows one to focus more on the battery aging minimization instead of on guaranteeing satisfactory driving performances. Therefore, in terms of control actions, this leads to lower  $DoD$  values, which reduce the driving range, and to a lower  $I_{max}^{cell}$ , which increases both the charging time and the error between the driver's desired speed and the actual vehicle velocity. Eventually, for a reasonable trade-off, a value of  $\alpha_l = 2.7 \times 10^8$  (km/Ah), in correspondence of the Pareto fronts elbows, is chosen.

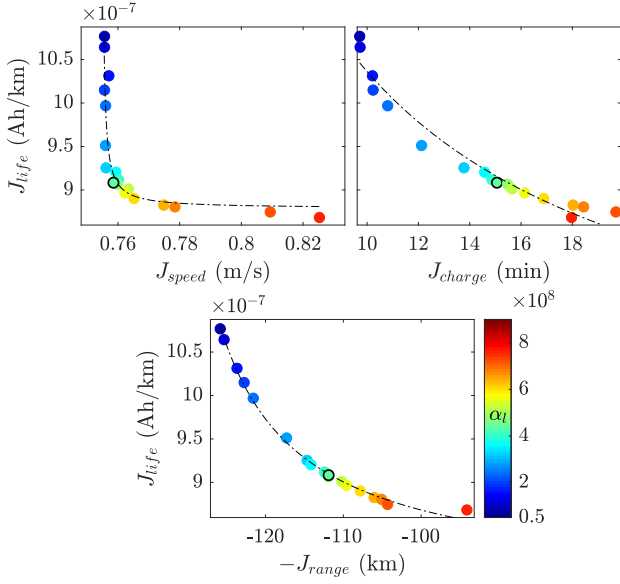


Fig. 10. Pareto front analysis for  $\alpha_l$  varying between  $5 \times 10^7$  and  $9 \times 10^8$  (km/Ah). Weights for  $J_{speed}$ ,  $J_{charge}$ , and  $J_{range}$  are constant over the analysis. Black edge colored circles highlight the solution for  $\alpha_l = 2.7 \times 10^8$  (km/Ah).

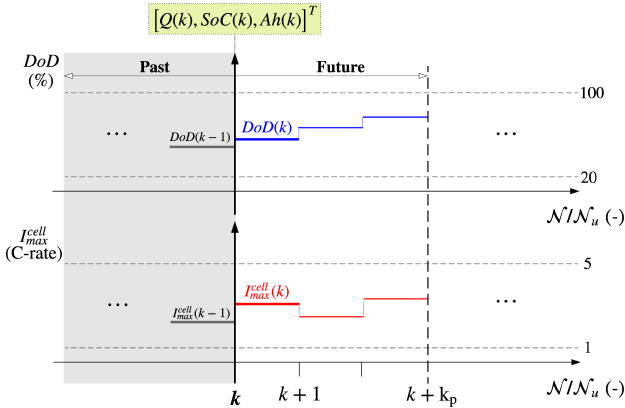


Fig. 11. Online optimization. At  $k$ , the objective function is minimized over a prediction horizon  $\mathcal{N}_p$  assuming a control discretization step  $\mathcal{N}_u$ . Only the control input computed from  $k$  to  $k+1$  is applied, before rerunning the optimization at  $k+1$ .

## B. Online Optimization

The offline optimization is carried out under the assumption of complete knowledge of the driver's behavior along the traveled distance  $\mathcal{N}$ . This makes the result not applicable in practice, here we introduce the online optimization technique. As summarized by Fig. 11, the idea is to introduce a Model Predictive Control (MPC) like procedure based on PSO. First, a prediction horizon  $\mathcal{N}_p$  and a control discretization step  $\mathcal{N}_u$  are selected, on a distance base, satisfying the following inequality:  $\mathcal{N}_u \leq \mathcal{N}_p$ . Therefore, at each optimization step  $k$ , with  $k$  the MPC index, the  $k_p = \mathcal{N}_p / \mathcal{N}_u$  future control variables are selected simulating the model over a prediction horizon  $\mathcal{N}_p$  while minimizing the

following reformulation of the cost function (24):

$$\begin{aligned}
 J_k = & \alpha_l \frac{Q(k) - Q(k + k_p)}{\mathcal{N}_p} \\
 & + \alpha_s \sqrt{\frac{1}{t(k + k_p) - t(k)} \int_{t(k)}^{t(k+k_p)} (v_{ref}(\tau) - v(\tau))^2 d\tau} \\
 & + \alpha_c \sqrt{\frac{1}{\mathcal{E}(k + k_p) - \mathcal{E}(k)} \sum_{i=\mathcal{E}(k)}^{\mathcal{E}(k+k_p)} t_c(i)^2} \\
 & - \alpha_r \sqrt{\frac{1}{\mathcal{E}(k + k_p) - \mathcal{E}(k)} \sum_{i=\mathcal{E}(k)}^{\mathcal{E}(k+k_p)} d_r(i)^2} \quad (29)
 \end{aligned}$$

where  $t(k + k_p) - t(k)$  is the time to travel  $\mathcal{N}_p$  kilometers and  $\mathcal{E}(k + k_p) - \mathcal{E}(k)$  the number of charging events between  $k$  and  $k + k_p$ . The minimization of (29) is still obtained relying on PSO. Therefore, only the first pair of control inputs  $[DoD(k), I_{max}^{cell}(k)]^T$  is applied from  $k$  to  $k+1$  (i.e., over a traveled distance  $\mathcal{N}_u$ ). The system state at  $k$ , provided as input for the prediction, takes the following form:

$$[Q(k), SoC(k), Ah(k)]^T \quad (30)$$

where  $Q(k)$ ,  $SoC(k)$ , and  $Ah(k)$  are respectively the residual capacity, the battery  $SoC$ , and the  $Ah$  processed till  $k$ . Note that this yields a closed-loop term. Eventually, the next optimization step is performed at  $k+1$ .

Since for each optimization step a prediction over  $\mathcal{N}_p$  is needed, an estimate of the future driver's behavior, in terms of desired speed, is necessary. We consider two cases. The *Online* approach assumes the *Artemis Rural* driving cycle to be a description of the average driver's behavior. In this case, the prediction over  $\mathcal{N}_p$  is the repetition of the aforementioned driving cycle; the driving cycle is applied regardless of the actual driving style. The *Online MC* approach on the other hand tries to consider the current drive style. It relies on the Markov chain model. It uses the online learnt transition matrix to generate the desired speed profile over  $\mathcal{N}_p$ . This second approach thus adapts to changes in the driving style. Fig. 12 summarizes the online optimization architecture.

As already mentioned, at each step  $k$ , the strategies solve an optimization over  $\mathcal{N}_p$ . A careful selection of prediction horizon and control discretization step is fundamental to solve the optimization problem in a reasonable time, without affecting the found strategy. In the following, we use  $\mathcal{N}_p = 6000$  (km) and  $\mathcal{N}_u = 2000$  (km) together with a particle swarm size  $p_{\#,2} = 60$ . The next section better illustrates the validity of the choice.

## V. RESULTS

To guarantee repeatability and fairness of comparison, the validation uses two deterministic driving styles: (a) the *Artemis Rural* driving cycle and (b) the *Highway Fuel Economy Test*, both illustrated in Fig. 13. Note that the *Highway Fuel Economy Test* is scaled in order to reach a maximum speed of 120 (km/h), a realistic speed limit in the European Union. The two driving cycles have complementary characteristics, the *Artemis Rural* has a lower average speed but a higher maximum acceleration



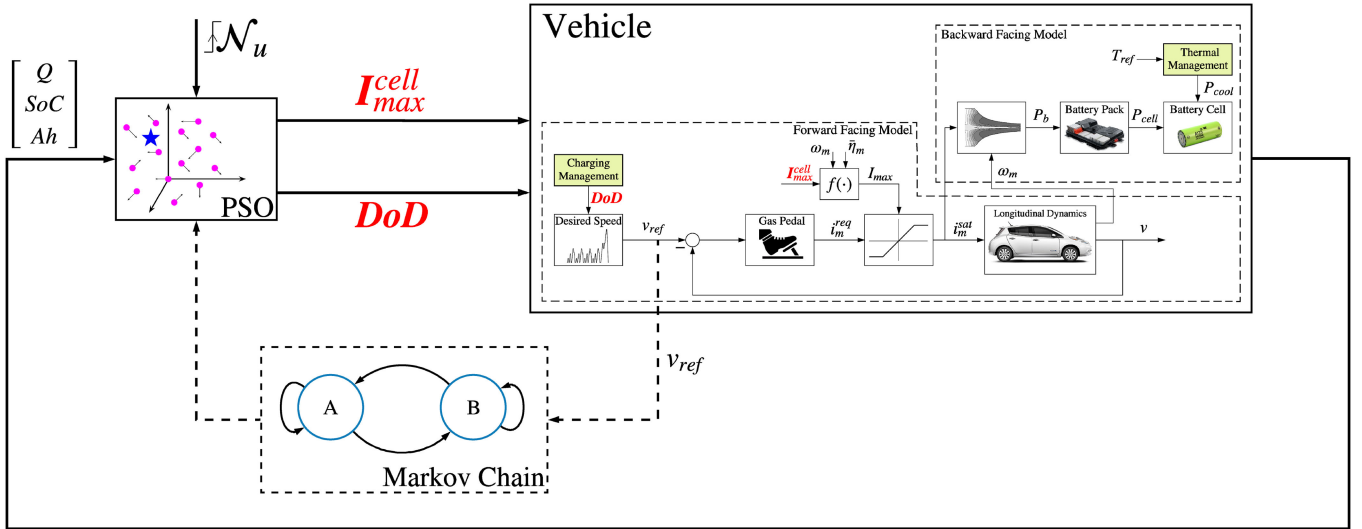


Fig. 12. Online optimization architecture. The first approach assumes the *Artemis Rural* driving cycle to be a good description of the driver's model. Thus, the Markov chain branch (dashed line) is deactivated. Conversely, the second approach relies on Markov chains to first learn the driver's behavior and then to generate the desired speed profile over the prediction horizon  $\mathcal{N}_p$ . The online optimization is triggered each control discretization step  $\mathcal{N}_u$ .

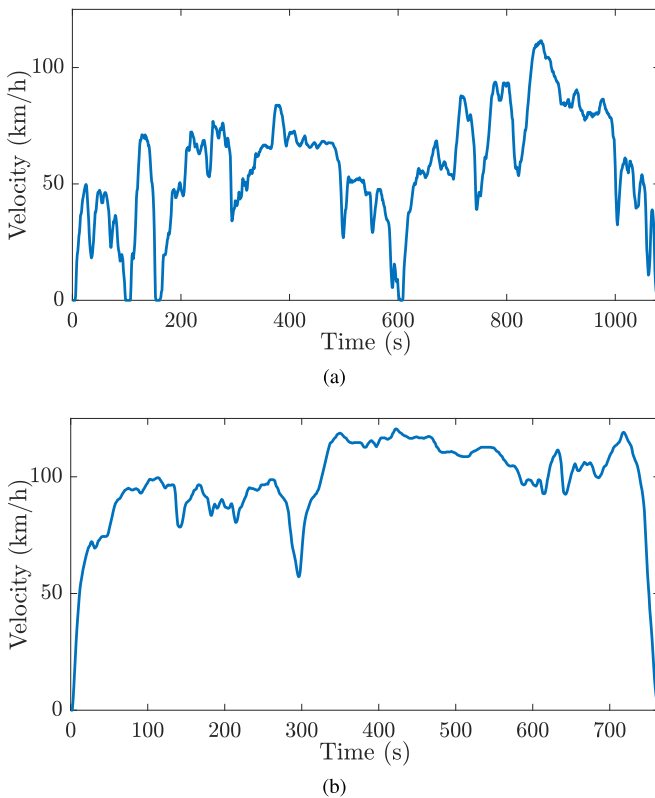


Fig. 13. *Artemis Rural* (a) and the *Highway Fuel Economy Test* (b) driving cycles.

than the *Highway Fuel Economy Test*; the *Artemis Rural* captures a more dynamic driving style, comprising both urban, and highway driving.

Figures 14 and 15 show the results for the *Artemis Rural* and the *Highway Fuel Economy Test* driving cycles in the time domain for different strategies. Table II summarizes the value

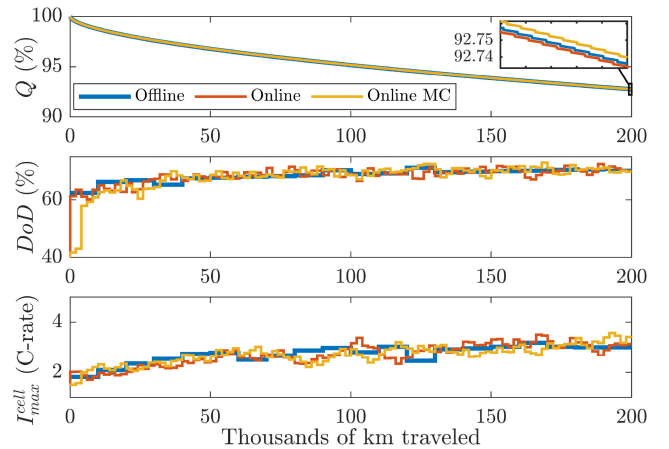


Fig. 14. *Artemis Rural* optimization results. The offline solution is compared to the *Online* and to the *Online MC* outcomes. To ease reader's comprehension, the final values for the battery capacity  $Q$ , obtained with the different policies, are highlighted.

of the cost functions. The table also computes the cost function for the open-loop case with no active battery degradation management strategy, see Appendix A. The comparison considers a horizon  $\mathcal{N}$  of 200 thousand kilometers, over which the driver's behavior is assumed to be fixed (i.e., either scenario (a) or (b), exclusively). From these results, one can draw the following conclusions for the *Artemis Rural* driving cycle:

- As expected, the offline benchmark, computed under the assumption of complete knowledge of the driver's behavior, achieves the best results for  $J$ . However, the offline policy leads to a slightly increased aging if compared to the *Online MC* solution. This is reasonable because the offline benchmark is the best trade-off between the different objectives and not the optimal solution from just an aging standpoint;

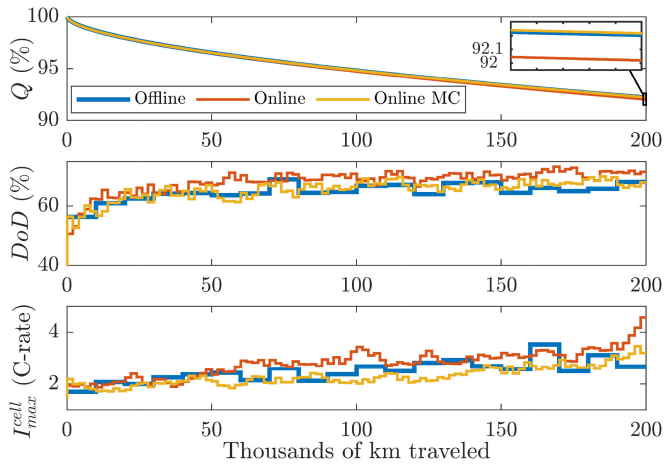


Fig. 15. Highway Fuel Economy Test optimization results. The offline solution is compared to the *Online* and to the *Online MC* outcomes. To ease reader's comprehension, the final values for the battery capacity  $Q$ , obtained with the different policies, are highlighted.

TABLE II  
OPTIMIZATION RESULTS. ONLINE AND OFFLINE SOLUTIONS ARE COMPARED TO AN OPEN-LOOP STRATEGY CHARACTERIZED BY  $DoD = 70\%$  AND  $I_{MAX}^{cell} = 2.5$  (C-RATE)

	Offline	Online	Online MC	Open-loop
Artemis Rural				
$Q$ (%)	92.736	92.733	92.740	92.645
$J$ (-)	223.792	224.278	224.742	225.770
$J_{life}$ (Ah/km)	$9.084 \times 10^{-7}$	$9.084 \times 10^{-7}$	$9.078 \times 10^{-7}$	$9.197 \times 10^{-7}$
$J_{speed}$ (m/s)	0.758	0.759	0.759	0.756
$J_{charge}$ (min)	14.765	15.060	14.713	16.001
$J_{range}$ (km)	112.008	111.885	110.956	114.134
Opt. time	2/3 weeks	20 (min/step)	25 (min/step)	NA*
Highway Fuel Economy Test				
$Q$ (%)	92.199	92.020	92.217	91.926
$J$ (-)	260.004	261.432	260.398	264.124
$J_{life}$ (Ah/km)	$9.753 \times 10^{-7}$	$9.976 \times 10^{-7}$	$9.732 \times 10^{-7}$	$10.095 \times 10^{-7}$
$J_{speed}$ (m/s)	0.575	0.574	0.577	0.573
$J_{charge}$ (min)	15.240	14.550	16.671	15.904
$J_{range}$ (km)	76.070	79.874	76.769	81.603
Opt. time	2/3 weeks	17 (min/step)	20 (min/step)	NA*

\*NA: Not Applicable.

- For the *Artemis Rural* driving cycle, both the *Online* and the *Online MC* strategies lead to results close to the offline benchmark. As a matter of fact, the *Online* solution is computed assuming the future driver's behavior to be modeled as an *Artemis Rural* driving cycle, which is the truth for this first study. The learning mechanism in this context does not bring any advantage. If anything, it actually leads to slightly worse performances. The loss of performance is due to the non perfect description of the driving cycle that the Markov chains achieves;
- The open-loop strategy leads to the worst results, with a lower residual battery capacity  $Q$  and a higher value for the objective function  $J$ .

On the other hand, the *Highway Fuel Economy Test* outlines different features:

- The open-loop approach is the worst also for this driving cycle;
- The *Online* strategy, which wrongly operates under the assumption of an *Artemis Rural* driving cycle, yields unsatisfactory results. This underlines the impact that the driving cycle has on the aging dynamics and consequently on the optimal strategy;
- The *Online MC* strategy introduces visible benefits. The learning mechanism allows for an adaptation to the driver's behavior, leading to results close to the offline benchmark. As a matter of fact, provided the residual battery capacity of the offline solution to be 92.199%, the *Online*, the *Online MC*, and the open-loop strategies lead respectively to: 92.020%, 92.217%, and 91.926%;
- Fig. 15 shows that the *Online* strategy employs higher  $DoD$  and  $I_{max}^{cell}$  than the offline and the *Online MC* solutions.

Both the *Online* and the open-loop strategies show high sensitivity with respect to the driver's behavior. Conversely, the *Online MC* is robust to modifications of the driving style. The *Online MC* approach leads to results close to the offline benchmark with an average optimization step time of 25 (min) for scenario (a), a reasonable computational time for the low dynamics under investigation and over a control discretization step  $\mathcal{N}_u = 2000$  (km). Indeed, 25 (min) corresponds to an average traveled distance of 24 (km), which is negligible for aging monitoring purposes.<sup>2</sup> Furthermore, the average computational time decreases with the increment of the driving cycle average speed. This is reasonable because, at each PSO optimization step, the model is simulated over  $\mathcal{N}_p$  for  $p_{\#,2}$  different configurations of the control variables  $DoD$  and  $I_{max}^{cell}$ . Thus, the higher the average velocity the quicker the simulation. The complexity introduced by the Markov-chain-based learning mechanism, in terms of computational time increment with respect to the *Online* strategy, is acceptable. Eventually, it must be noted that, while the proposed online strategies are demanding in terms of computational power, there is not hard real time constraints that would force a local computation. As a matter of fact, given the slow dynamics of battery aging, and the rising trend in interconnected vehicles, the optimal battery management strategy can be computed relying on cloud services without any computational power limitation.

Table II, while showing that the proposed approach is capable of improving the cost function and reducing battery aging, also shows that the absolute gain with respect to the open-loop strategy is not very large. Extrapolating the results to a battery end of life equivalent to 80% the gain in terms of vehicle life extension is 18,000 (km). In interpreting these results, one should consider two important points:

- The open-loop strategy (as shown in Appendix) is itself the result of an optimization. If a  $DoD$  of 75% is used instead of the optimal one, the gain in terms of kilometers grows to 48,000 (km);

<sup>2</sup>Solutions of offline and online optimizations were computed on a Intel Core i7-7700HQ processor with 16.0 (GB) of RAM.

- The proposed strategy is also adaptive. This means that the Markov chain is capable of adapting to modifications of the driver's behavior, thus increasing robustness.

## VI. CONCLUSION

The paper proposes a strategy for battery aging management for EV's. Battery aging management in electric vehicles is particularly complex because it entails a modification of the vehicle performance.

The first part of the paper introduces the main features and specifics of the problem. A mixed forward/backward electric vehicle model defines the main stress factors affecting battery aging and with them the control variables. Subsequently, these results inform the definition of a cost function that quantifies battery aging along with the loss of performance. The optimization problem is first solved offline relying on PSO. Then, we propose two online aging management strategies. Both employ a receding horizon approach, in the first case the horizon is computed assuming a constant driving cycle, whereas the second case uses a self-learning Markov chain parametrization of the driving cycle. This allows for an adaptation.

The paper shows that active aging management can extend the life of the EV. Relying on a Markov chain description of the driving style, the main advantage of the proposed online approach is its capability to adapt to modifications of the driver's behavior. Thus, the use of the proposed active aging management would reduce the maintenance cost of EV's reduce the risk of possible replacements of the battery pack during the vehicle lifetime. Future works will extend the proposed framework focusing on scenarios characterized by model uncertainties and nonlinear fading.

## APPENDIX A

The open-loop strategy is obtained testing feasible  $(DoD, I_{max}^{cell})$  combinations, such that  $DoD \in \{20, 100\}\%$  and  $I_{max}^{cell} \in \{1, 5\}$  (C-rate). Each control inputs couple is assumed to be constant over a horizon of 200 thousand kilometers. Therefore, for each couple, the performance index (24) is computed and Fig. 16 is obtained. The control variables associated with the minimum value for the cost function  $J$  are chosen as the open-loop benchmark for Section V. Assuming the *Artemis Rural* driving cycle to be a good average description of the driver's desired speed,  $DoD = 70\%$  and  $I_{max}^{cell} = 2.5$  (C-rate) lead to the minimum open-loop value of the objective function.

## REFERENCES

- [1] E. Helmers and P. Marx, "Electric cars: Technical characteristics and environmental impacts," *Environ. Sci. Eur.*, vol. 24, no. 1, 2012, Art. no. 14.
- [2] L. Lu, X. Han, J. Li, J. Hua, and M. Ouyang, "A review on the key issues for lithium-ion battery management in electric vehicles," *J. Power Sources*, vol. 226, pp. 272–288, 2013.
- [3] A. Barré, B. Deguilhem, S. Grolleau, M. Gérard, F. Suard, and D. Riu, "A review on lithium-ion battery ageing mechanisms and estimations for automotive applications," *J. Power Sources*, vol. 241, pp. 680–689, 2013.
- [4] W. Bögel, J. P. Büchel, and H. Katz, "Real-life EV battery cycling on the test bench," *J. Power Sources*, vol. 72, no. 1, pp. 37–42, 1998.
- [5] K. Amine *et al.*, "Factors responsible for impedance rise in high power lithium ion batteries," *J. Power Sources*, vol. 97, pp. 684–687, 2001.

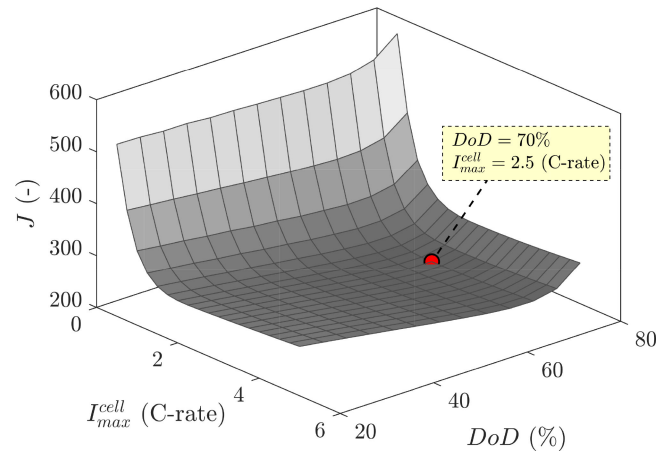


Fig. 16. *Artemis Rural* open-loop results.  $DoD = 70\%$  and  $I_{max}^{cell} = 2.5$  (C-rate) lead to the minimum open-loop value of the objective function.

- [6] S. Zhang, K. Xu, and T. Jow, "Electrochemical impedance study on the low temperature of li-ion batteries," *Electrochimica Acta*, vol. 49, no. 7, pp. 1057–1061, 2004.
- [7] I. Baghdadi, O. Briat, J.-Y. Delétage, P. Gyan, and J.-M. Vinassa, "Lithium battery aging model based on dakin's degradation approach," *J. Power Sources*, vol. 325, pp. 273–285, 2016.
- [8] J. Wang *et al.*, "Cycle-life model for graphite-LiFePO<sub>4</sub> cells," *J. Power Sources*, vol. 196, no. 8, pp. 3942–3948, 2011.
- [9] G. Suri and S. Onori, "A control-oriented cycle-life model for hybrid electric vehicle lithium-ion batteries," *Energy*, vol. 96, pp. 644–653, 2016.
- [10] M. Ecker *et al.*, "Calendar and cycle life study of Li (NiMnCo) O<sub>2</sub>-based 18650 lithium-ion batteries," *J. Power Sources*, vol. 248, pp. 839–851, 2014.
- [11] J. Jaguemont, L. Boulon, and Y. Dubé, "A comprehensive review of lithium-ion batteries used in hybrid and electric vehicles at cold temperatures," *Appl. Energy*, vol. 164, pp. 99–114, 2016.
- [12] X. Hu, C. M. Martinez, and Y. Yang, "Charging, power management, and battery degradation mitigation in plug-in hybrid electric vehicles: A unified cost-optimal approach," *Mech. Syst. Signal Process.*, vol. 87, pp. 4–16, 2017.
- [13] S. Ebbesen, P. Elbert, and L. Guzzella, "Battery state-of-health perceptible energy management for hybrid electric vehicles," *IEEE Trans. Veh. Technol.*, vol. 61, no. 7, pp. 2893–2900, Sep. 2012.
- [14] L. Serrao, S. Onori, A. Sciarretta, Y. Guezennec, and G. Rizzoni, "Optimal energy management of hybrid electric vehicles including battery aging," in *Proc. IEEE Amer. Control Conf.*, 2011, pp. 2125–2130.
- [15] G. Pozzato, S. Formentin, G. Panzani, and S. M. Savaresi, "Least costly energy management for extended range electric vehicles with start-up characterization," in *Proc. IEEE Conf. Control Technol. Appl.*, 2018, pp. 1020–1025.
- [16] S. Formentin, J. Guanetti, and S. M. Savaresi, "Least costly energy management for series hybrid electric vehicles," *Control Eng. Pract.*, vol. 48, pp. 37–51, 2016.
- [17] G. Pozzato, S. Formentin, G. Panzani, and S. M. Savaresi, "Least costly energy management for extended-range electric vehicles with noise emissions characterization," in *Proc. 9th Int. Symp. Adv. Automot. Control*, 2019, pp. 586–591.
- [18] K. W. E. Cheng, B. Divakar, H. Wu, K. Ding, and H. F. Ho, "Battery-management system (BMS) and SOC development for electrical vehicles," *IEEE Trans. Veh. Technol.*, vol. 60, no. 1, pp. 76–88, Jan. 2011.
- [19] M. A. Hannan, M. H. Lipu, A. Hussain, and A. Mohamed, "A review of lithium-ion battery state of charge estimation and management system in electric vehicle applications: Challenges and recommendations," *Renew. Sustain. Energy Rev.*, vol. 78, pp. 834–854, 2017.
- [20] M. M. U. Rehman, F. Zhang, M. Evzelman, R. Zane, K. Smith, and D. Maksimovic, "Advanced cell-level control for extending electric vehicle battery pack lifetime," in *Proc. IEEE Energy Convers. Congr. Expo.*, 2016, pp. 1–8.

- [21] X. Hu, J. Jiang, D. Cao, and B. Egardt, "Battery health prognosis for electric vehicles using sample entropy and sparse Bayesian predictive modeling," *IEEE Trans. Ind. Electron.*, vol. 63, no. 4, pp. 2645–2656, Apr. 2016.
- [22] K. S. Ng, C.-S. Moo, Y.-P. Chen, and Y.-C. Hsieh, "Enhanced Coulomb counting method for estimating state-of-charge and state-of-health of lithium-ion batteries," *Appl. Energy*, vol. 86, no. 9, pp. 1506–1511, 2009.
- [23] S. J. Moura, N. A. Chaturvedi, and M. Krstić, "Adaptive partial differential equation observer for battery state-of-charge/state-of-health estimation via an electrochemical model," *J. Dyn. Syst., Meas., Control*, vol. 136, no. 1, 2014, Art. no. 011015.
- [24] S. Sabatini and M. Corno, "Battery aging management for fully electric vehicles," in *Proc. IEEE Eur. Control Conf.*, 2018, pp. 231–236.
- [25] J. G. Hayes and K. Davis, "Simplified electric vehicle powertrain model for range and energy consumption based on EPA coast-down parameters and test validation by argonne national lab data on the nissan leaf," in *Proc. Transp. Electrification Conf. Expo.*, 2014, pp. 1–6.
- [26] S. Onori, L. Serrao, and G. Rizzoni, *Hybrid Electric Vehicles: Energy Management Strategies*. London, U.K.: Springer, 2016.
- [27] J. Schmalstieg, S. Käbitz, M. Ecker, and D. U. Sauer, "A holistic aging model for Li (NiMnCo) O<sub>2</sub> based 18650 lithium-ion batteries," *J. Power Sources*, vol. 257, pp. 325–334, 2014.
- [28] S. F. Schuster, M. J. Brand, C. Campestrini, M. Gleissenberger, and A. Jossen, "Correlation between capacity and impedance of lithium-ion cells during calendar and cycle life," *J. Power Sources*, vol. 305, pp. 191–199, 2016.
- [29] X. Lin *et al.*, "A lumped-parameter electro-thermal model for cylindrical batteries," *J. Power Sources*, vol. 257, pp. 1–11, 2014.
- [30] T. Malik and C. Bullard, "Air conditioning hybrid electric vehicles while stopped in traffic," Air Conditioning and Refrigeration Center. Univ. Illinois Mech. Ind. Eng. Dept., College of Engineering, Tech. Rep., 2004.
- [31] S. Bauer, A. Suchanek, and F. P. León, "Thermal and energy battery management optimization in electric vehicles using pontryagin's maximum principle," *J. Power Sources*, vol. 246, pp. 808–818, 2014.
- [32] Y. Masoudi, A. Mozaffari, and N. L. Azad, "Battery thermal management of electric vehicles: An optimal control approach," in *Proc. ASME Dyn. Syst. and Control Conf.*, 2015, pp. 4365–4370.
- [33] M. André, "The artemis european driving cycles for measuring car pollutant emissions," *Sci. Total Environ.*, vol. 334, pp. 73–84, 2004.
- [34] F. Lambert, "Tesla battery data shows path to over 500,000 miles on a single pack," 2016. [Online]. Available: <https://electrek.co/2016/11/01/tesla-battery-degradation/>
- [35] S. Di Cairano, D. Bernardini, A. Bemporad, and I. V. Kolmanovskiy, "Stochastic MPC with learning for driver-predictive vehicle control and its application to HEV energy management," *IEEE Trans. Contr. Sys. Techn.*, vol. 22, no. 3, pp. 1018–1031, May 2014.
- [36] Y. Zou, Z. Kong, T. Liu, and D. Liu, "A real-time Markov chain driver model for tracked vehicles and its validation: Its adaptability via stochastic dynamic programming," *IEEE Trans. Veh. Technol.*, vol. 66, no. 5, pp. 3571–3582, May 2017.
- [37] T.-K. Lee, B. Adornato, and Z. S. Filipi, "Synthesis of real-world driving cycles and their use for estimating phev energy consumption and charging opportunities: Case study for midwest/us," *IEEE Trans. Veh. Technol.*, vol. 60, no. 9, pp. 4153–4163, Nov. 2011.
- [38] S. Ebbesen, P. Kiwiz, and L. Guzzella, "A generic particle swarm optimization Matlab function," in *Proc. IEEE Amer. Control Conf.*, 2012, pp. 1519–1524.



**Matteo Corno** received the M.Sc. degree in computer and electrical engineering from the University of Illinois, Champaign, IL, USA, and the Ph.D. cum laude degree with a thesis on active stability control of two-wheeled vehicles from the Politecnico di Milano, Milano, Italy, in 2005 and 2009. He is an Associate Professor with the Dipartimento di Elettronica, Informazione e Bioingegneria, Politecnico di Milano, Italy. He held research positions at Thales Alenia Space, Harley Davidson, University of Minnesota, Johannes Kepler University in Linz, and TU Delft. His current research interests include dynamics and control of vehicles (especially electric-hybrid vehicles), Lithium-ion battery modeling, estimation and control.



**Gabriele Pozzato** was born in Vicenza, Italy, on October 31st 1991. He received the bachelor's degree in information engineering from Università di Padova, Padova, Italy, and the M.Sc. (cum laude) in automation and control engineering from Politecnico di Milano, Milano, Italy, defending a thesis on analysis and development of slip and launch control systems for a high-performance motorcycle. He is currently working toward the Ph.D. degree at the Politecnico di Milano. The main focus of his doctoral research is the optimization and control of vehicles' powertrain.

He was a visiting scholar with the Clemson University International Center for Automotive Research, Greenville, SC, USA, from January to November, 2016.